

# Geophysical Research Letters

## RESEARCH LETTER

10.1029/2019GL085377

### Key Points:

- We propose an approach to quantify the ratio between elastic and inelastic deformation in subduction forearcs
- Two distinct correlations can be observed between interseismic and Quaternary uplift rates
- We propose that 4% to 8% of interseismic uplift rates translate into persistent deformation in northern Chile

### Supporting Information:

- Supporting Information S1

### Correspondence to:

R. Jolivet,  
romain.jolivet@ens.fr

### Citation:

Jolivet R., Simons, M., Duputel, Z., Olive, J.-A., Bhat, H. S., & Bleiter, Q. (2020). Interseismic loading of subduction megathrust drives long-term uplift in Northern Chile. *Geophysical Research Letters*, 47, e2019GL085377. <https://doi.org/10.1029/2019GL085377>

Received 11 SEP 2019

Accepted 2 APR 2020

Accepted article online 9 APR 2020

## Interseismic Loading of Subduction Megathrust Drives Long-Term Uplift in Northern Chile

**R. Jolivet<sup>1,2</sup> , M. Simons<sup>3</sup> , Z. Duputel<sup>4</sup> , J.-A. Olive<sup>1</sup> , H. S. Bhat<sup>1</sup> , and Q. Bleiter<sup>5</sup> **

<sup>1</sup>Laboratoire de Géologie, Département de Géosciences, École Normale Supérieure, PSL Université, CNRS UMR 8538, Paris, France, <sup>2</sup>Institut Universitaire de France, Paris, France, <sup>3</sup>Seismological Laboratory, California Institute of Technology, Pasadena, CA, USA, <sup>4</sup>Institut de Physique du Globe de Strasbourg, Université de Strasbourg/EOST, CNRS UMR 7516, Strasbourg, France, <sup>5</sup>Université Côte d'Azur, IRD, CNRS, Observatoire de la Côte d'Azur, Géoazur, Sophia Antipolis, France

**Abstract** Large earthquakes are the product of elastic stress that has accumulated over decades to centuries along segments of active faults. Assuming an elastic crust, one can roughly estimate the location and rate of accumulation of elastic stress. However, this general framework does not account for inelastic, irrecoverable deformation, which results in large-scale topography. We do not know over which part of the earthquake cycle such deformation occurs. Using InSAR and GNSS measurements, we report on a potential correlation between long-term, inelastic vertical rate and short-term, interseismic vertical rate in northern Chile. Approximately 4% to 8% of the geodetically derived interseismic vertical rates translate into permanent deformation, suggesting that topography of the forearc builds up during the interseismic period. This observation provides a quantitative basis for an improved understanding of the interplay between short-term and long-term dynamics along convergent plate boundaries.

## 1. Introduction

Along a subduction interface, the quasicontinuous motion of converging plates leads to the build up of elastic stress where the interface is locked (Savage, 1983). Large earthquakes, occurring as slip on the megathrust interface, redistribute elastic energy accumulated within the surrounding medium. In addition to these sudden changes in stress, parts of the subduction interface may slip aseismically during the interseismic period, either episodically during slow slip events (Dragert et al., 2001; Hirose et al., 1999) or over decades to centuries (Mazzotti et al., 2000; Metois et al., 2016). Averaged over the interseismic period, a coupling coefficient,  $\gamma$ , is usually used to describe the inferred local slip deficit normalized by the long-term convergence rate along the subduction megathrust (Figure 1).  $\gamma = 1$  corresponds to a fully locked interface, with a potential for slip during future earthquakes.  $\gamma = 0$  indicates an inferred slip rate equal to the local plate convergence rate (Savage, 1983). Subduction interfaces are paved with locked sections (i.e., portions of the interface with  $\gamma \approx 1$ ) separated by sections that slip aseismically (e.g., Freymueller & Beavan, 1999; Nocquet et al., 2014; Pritchard et al., 2006) (i.e.,  $\gamma \ll 1$ ).

Large megathrust earthquakes uplift the surface located above a patch of slip and induce subsidence around it (e.g., Savage, 1983; Simons et al., 2011; Vigny et al., 2011). To the extent that the coupling coefficient,  $\gamma$ , is stable through time, segments that ruptured during a large event reload during the interseismic period causing surface deformation of opposite sign to that occurring during the earthquake. In the most simplistic model, the amount of slip during earthquakes should be balanced by the slip deficit that builds up in the interim period, at least once integrated over many earthquake cycles. However, along several subduction zones, the coastal domain, a region defined to extend from the coast to the continental shelf (Figure 1), experiences long-lived vertical displacement, either subsidence or uplift, over geological times (i.e.,  $10^5$ – $10^6$  years), for example, as inferred from the geometry of raised terraces in Chile (Regard et al., 2010; Saillard et al., 2009), Japan (Matsu'ura, 2015), or Greece (Mouslopoulou et al., 2016) or the erosion patterns along rivers in Mexico (Ramírez-Herrera et al., 2018). Such long-term, irrecoverable deformation can be modeled with a purely plastic rheology, for instance, using critical taper theory (Davis et al., 1983). Such models, however, cannot address the question of when inelastic deformation cumulates in the forearc with respect to the different phases of the earthquake cycle.

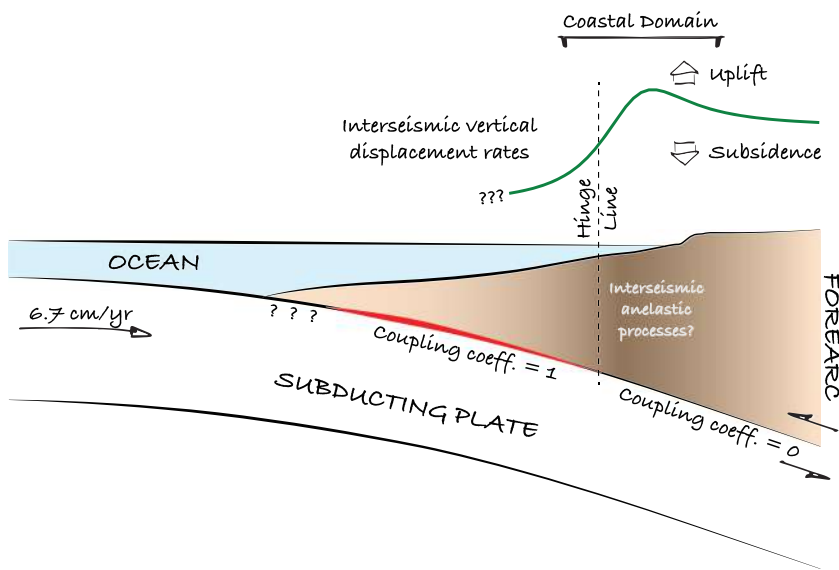


**Figure 1.** Simplified seismotectonic setting of the subduction forearc—An oceanic plate slides underneath the subduction forearc. The interface is divided between a locked section and an, unlocked section. The coupling coefficient is the parameter describing the apparent slip deficit normalized by the long-term plate convergence rate. A coupling coefficient of 0 indicates slip at plate rate along the interface while a coupling coefficient of 1 indicates full kinematic locking. The coastal domain is the region proximal to the coastline that is submitted to changes in sea level. During the interseismic period, uplift is maximum at the hinge line, which corresponds to the surface projection of the transition between the locked and unlocked sections of the interface at depth.

For comparison, typical vertical displacement rates over geological times for the coastal domain are generally one order of magnitude lower than typical interseismic uplift or subsidence rates (a fraction of millimeter per year vs several millimeters per year, e.g., Figure 1 Béjar-Pizarro et al., 2013; Hashima & Sato, 2017; Jolivet & Simons, 2018; Melnick, 2016; Regard et al., 2010). Comparatively, large megathrust earthquakes will generate meter-scale vertical displacements every time they occur (e.g., Simons et al., 2011; Vigny et al., 2011). We cannot yet assess exactly how much permanent uplift or subsidence occurs during earthquakes (Baker et al., 2013; Melnick, 2016) or during the interseismic period (Béjar-Pizarro et al., 2013; Saillard et al., 2017), as our understanding of the earthquake cycle is limited to simplified elastic and viscoelastic models, which do not allow for permanent deformation to build up within the upper crust.

Focusing on the interseismic period, correlations between distributions of coupling coefficients along megathrusts and morphotectonic features (Saillard et al., 2017; Victor et al., 2011) or large-amplitude gravity anomalies (Song & Simons, 2003; Wells et al., 2003) suggest that interseismic fault locking is to first order a long-term feature, stable over many seismic cycles. Interseismic fault locking is thought to imprint its signature in the morphology of the subduction forearc. For instance, a qualitative relationship has been described between the maximum depth of high coupling coefficient along subduction megathrust and the position of the coastal domain (Béjar-Pizarro et al., 2013; Mouslopoulou et al., 2016; Roussel et al., 2015; Saillard et al., 2017) (Figure 1). If part of the uplift measured during the interseismic period is not recovered elastically during earthquakes occurring along the megathrust, then anelastic deformation accumulates, and the coastal domain will uplift over geological times (Mouslopoulou et al., 2016; Saillard et al., 2017; Song & Simons, 2003). Because most of the slip is often located offshore, earthquakes along subduction zones tend to lower the coastal domain (Duputel et al., 2015; Simons et al., 2011). However, if coseismic slip reaches depths below the coastline, the coastal domain will uplift coseismically (Grandin et al., 2016; Vigny et al., 2011).

The residual permanent vertical displacement will therefore depend on the relative balance between coseismic slip and interseismic slip deficit and on the position of the hinge line with respect to the coastal domain (Saillard et al., 2017). Contradictory conclusions have been reached considering the contribution of earthquakes and interseismic loading to the permanent deformation of the forearc. For instance, Melnick (2016) proposes that intermediate-depth earthquakes are responsible for the uplift of the northern Chilean coast while he discards the influence of interseismic fault locking. Other studies point to spatial relationships

between patterns of coupling coefficients and long-term features of the forearc in support of the influence of interseismic fault locking on topography building (Béjar-Pizarro et al., 2013; Mouslopoulou et al., 2016; Rousset et al., 2015; Saillard et al., 2017).

## 2. Data and Methods: The Case of Northern Chile

Here, we use direct estimates of interseismic displacement rates and compare these with long-term uplift rates in subduction regions. Geodetic measurements of surface displacement rates, including GNSS (historically referred to as GPS) and Synthetic Aperture Radar Interferometry (InSAR) measurements, are available over many subduction forearcs. InSAR provides measurements of surface deformation along the direction of the line of sight (LOS) of a satellite. For SAR acquisitions from the Envisat satellite, for instance, the LOS incidence angle is approximately 23° resulting in a high sensitivity to vertical displacements. However, InSAR is also sensitive to horizontal displacements confounding attempts to isolate a purely vertical component of displacement. GNSS provides time series of three-component displacements at sparsely distributed locations. However, uncertainties on GNSS-derived vertical displacement rates typically reach several millimeters per year, making it a challenge to measure the submillimetric displacement rates expected from permanent deformation (Melnick, 2016).

One solution is to estimate a model of the distribution of coupling coefficients along the megathrust that captures all measurements of vertical, horizontal, and LOS displacements along with their respective uncertainties in order to produce an a posteriori estimate of vertical interseismic motion and compare those predictions with long-term displacement rates. Along subduction zones, where locking of the megathrust is mostly offshore, it is possible to infer locked asperities with geodetic measurements made onshore (e.g., Béjar-Pizarro et al., 2013; Lin et al., 2015). However, because we are generally limited to observations made at the surface and onshore, inferred distributions of coupling coefficient often differ significantly due to different modeling strategies and different regularizations of the inverse problem. In the present study, we do not particularly care about this nonuniqueness since we only use these models to provide the best possible estimate of vertical displacement rates over the interseismic period consistent with the available geodetic data. Effectively, models are used to interpolate the data.

Considering the duration of the modern instrumental period with respect to both the characteristic time of the earthquake cycle and the longer time required to accumulate significant anelastic deformation, it is crucial to focus on a region where we will be able to measure surface displacements that are unambiguously related to interseismic loading of the megathrust. In particular, the relaxation period following a large earthquake might extend over decades and could strongly influence what is considered as interseismic deformation (Hashima & Sato, 2017; Trubienko et al., 2013). Finally, this region must be densely sampled by GNSS measurements, and its geographical characteristics must be optimal for InSAR.

Northern Chile has been hit by several earthquakes, including the large,  $M_w$  7.7, Tocopilla earthquake (Bejar-Pizarro et al., 2010; Schurr et al., 2012) in 2007 and the great,  $M_w$  8.1, Iquique earthquake (Duputel et al., 2015) in 2014. There, inferences of along-strike variations of coupling coefficients are broadly consistent between models (Metois et al., 2016; Schurr et al., 2014). The last great megathrust event prior to the 2014 Iquique earthquake occurred in 1877 with an estimated magnitude of 8.6 (Comte & Pardo, 1991; Metois et al., 2013). Therefore, we assume that surface displacement rates in this region prior to the 2014 Iquique earthquake are not significantly changing due to postseismic viscous relaxation and truly reflect the effect of locking along the megathrust.

The relative aridity of northern Chile makes it an ideal target for InSAR measurements (e.g., Béjar-Pizarro et al., 2013; Pritchard & Simons, 2002). We use SAR data acquired by the Envisat satellite over the 2003–2010 period to derive a map of LOS ground velocity (Figure 2). We use a multipixel method to infer displacement time series, displacement rates averaged over the observation period, and earthquake-related offsets accounting for spatial covariances as well as other nuisance parameters (Jolivet & Simons, 2018). Our approach resolves long wavelength signals in SAR acquisitions, hence does not require input from GNSS data. The resulting map of LOS displacement rates highlights a variable uplift rate along the coastal domain, with LOS rates spanning a 0 to 4 mm/year range. Measurements of horizontal interseismic displacement rates are available thanks to the dense continuous GNSS measurements that have been deployed since 2000 (Simons et al., 2010) and are complementary to our InSAR displacement rate maps (Metois et al., 2016).

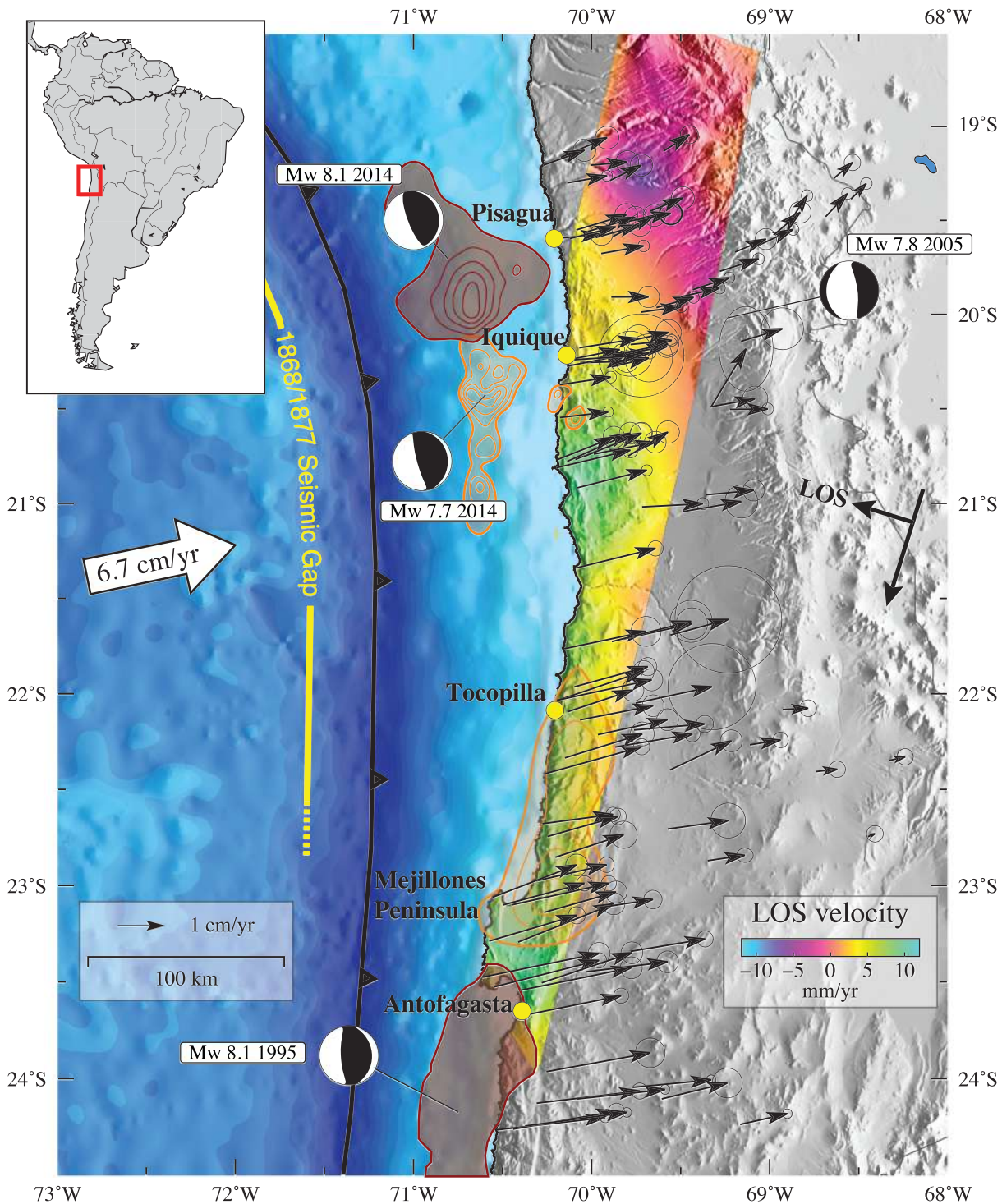


**Figure 2.** Tectonic setting and data set—Maps of the northern Chilean subduction zone. Arrows on the top map are GNSS-derived velocities from Metois et al. (2016) for the interseismic period preceding the 2014 earthquake. Color indicates ground velocity in the direction of the satellite line of sight for Envisat acquisitions along track 96 (Jolivet & Simons, 2018). Dark red contour lines are 2-m slip contours for earthquakes of magnitude larger than 8, including the Antofagasta, M<sub>w</sub> 8.1, 1995 event (Pritchard et al., 2002) and the Iquique, M<sub>w</sub> 8.1, 2014 event (Duputel et al., 2015). Orange contour lines are 0.5-m slip contours for earthquakes of magnitude between 7 and 8, including the 2007, M<sub>w</sub> 7.7, Tocopilla event (Béjar-Pizarro et al., 2013) and the 2014, M<sub>w</sub> 7.7, Iquique's biggest aftershock (Duputel et al., 2015). Focal mechanisms for earthquakes larger than Magnitude 7.5 since 1995 are from the Global CMT project (Ekström et al., 2012). Topography is from SRTM (Farr & Kobrick, 2000).

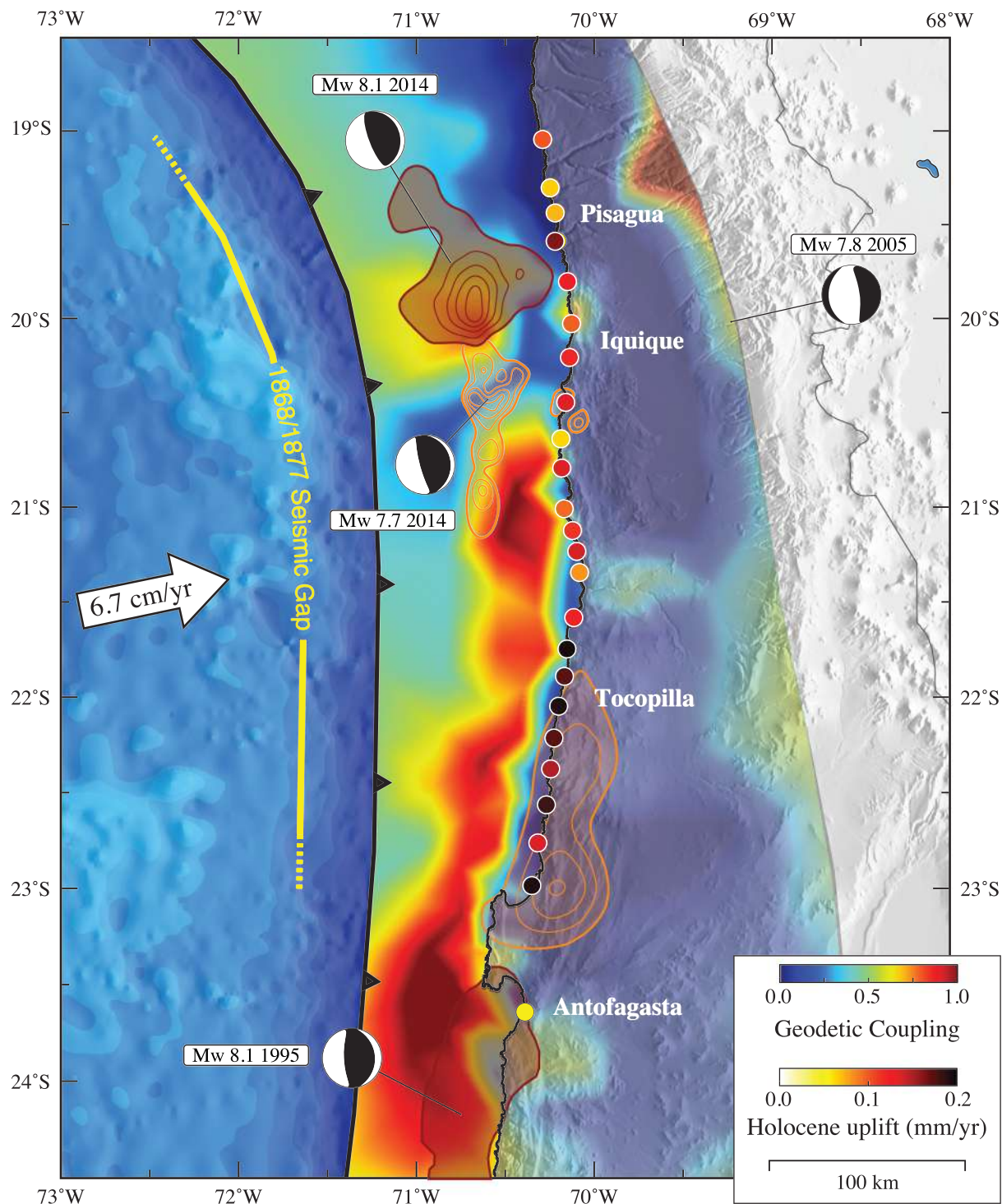


**Figure 3.** Megathrust coupling and slip distributions—Mean of the posterior PDF of the coupling coefficient along the megathrust. Color indicates whether the fault is kinematically coupled (red) or creeping at the plate rate (blue). Colored circles are the inferred Quaternary uplift rates from Melnick (2016). Earthquake slip distributions and moment tensors are similar as in Figure 2.

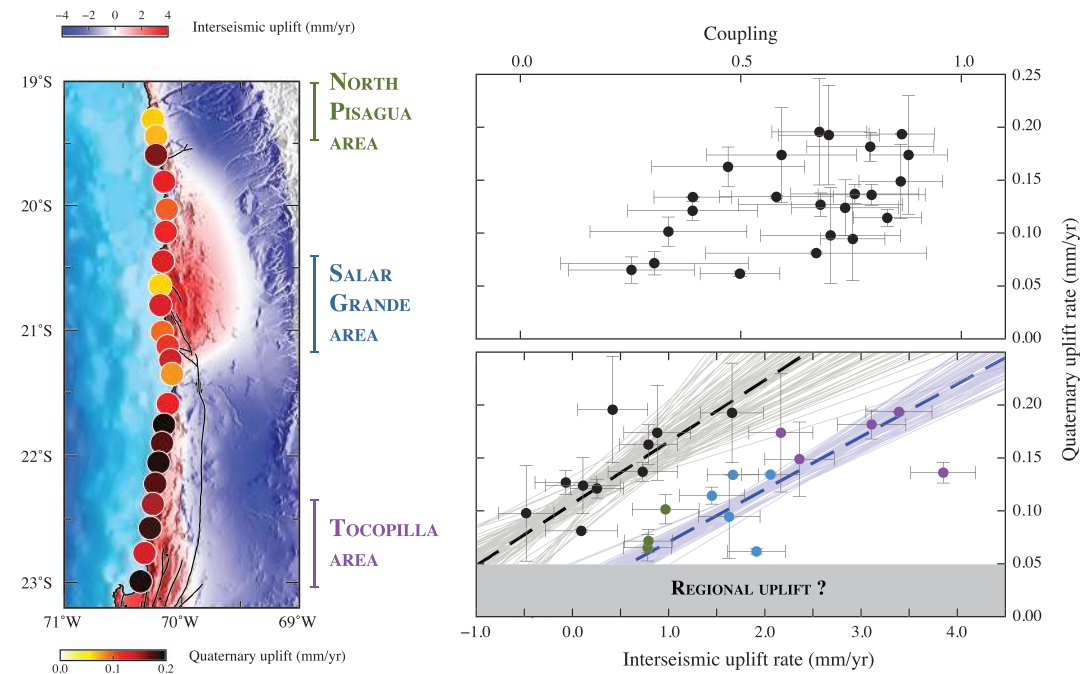


**Figure 4.** Comparison between short-term interseismic fault behavior and Quaternary coastal uplift—Map shows Quaternary coastal uplift rate (Melnick, 2016) (colored circles) and interseismic uplift rates predicted from our model (background color). (Top right) Quaternary coastal uplift as a function of coupling coefficient offshore, 50 km from the coast in a direction parallel to relative plate motion. (Bottom right) Quaternary coastal uplift as a function of interseismic uplift with our interpretation of the relationship between interseismic and Quaternary uplift. Colored dots indicate locations where Quaternary active faulting has been identified (please refer to the map for the location of these colored points Allmendinger & González, 2010). Thick blue and black lines are the linear trends predicted from the Bayesian regression for the region where Quaternary active faulting has been identified and not identified, respectively. Thin lines show a hundred realizations of the posterior PDF derived by the Bayesian regression, reflecting the range of possible trends for each group of points. See supporting information for a similar plot without interpretation, for a figure highlighting the position of the various points on a map, and for a description of the regression applied.

We use a backslip approach to estimate the coupling coefficient from geodetic displacement rates (Savage, 1983) and apply a Bayesian formalism to explore the range of possible models given the GNSS and InSAR surface rates (Jolivet et al., 2015). The mean interseismic coupling model is broadly consistent with the most recent published studies (Li et al., 2015; Metois et al., 2016). We infer a highly coupled segment extending northwards from, at least, Antofagasta in the south up to 20.5°S and a relatively less coupled segment offshore Iquique (Figure 3). The mean model has lower coupling coefficients at the trench, but this feature is not resolved given that we are limited to observations made onshore (see supporting information). There is a clear and robust separation between the coupled segments, with a narrow barrier with a coupling coefficient of 0 (a posteriori mean equals  $0.1 \pm 0.1$ ). Contrary to recently published models (Li et al., 2015; Metois et al., 2016), we do not infer fault locking underneath the south American continent. This inference of no kinematic locking extending below the coastline is driven by the InSAR observations indicating only onshore uplift (Béjar-Pizarro et al., 2013).

Our goal is to compare the short-term vertical displacements predicted by our coupling models to long-term estimates of coastal uplift. Figure 4 shows the vertical displacement rates over the forearc predicted by our mean coupling model. To first order, topography shows striking similarities with this pattern of vertical rates, as maximum uplift is located in the Coastal Cordillera. However, topography is a signal integrated over millions of years, amalgamating the effects of tectonics, mantle dynamics, and erosion. Therefore, topography alone cannot be simply used to study the influence of short-term megathrust dynamics on the building of topography.

The presence of marine terraces all along the Chilean coast documents the long-term uplift of the coastal domain over the Quaternary (Regard et al., 2010; Saillard et al., 2017). Using a landscape evolution model that accounts for variations in sea level to reproduce the topography of the coastal domain and, in particular,

the shape of the so-called coastal rasa, based on the competition of wave erosion and uniform uplift, Melnick (2016) determined uplift rates over the Quaternary with dense spatial sampling. These rates quantify the uplift of the Chilean coast at an average rate of  $0.13 \pm 0.04$  mm/year since, at least, 1 Myr.

Lateral variations within these Quaternary uplift rates are visible along the coast. Melnick (2016) finds no obvious correlation between the long-term rates and interseismic rates. However, the interseismic model used to predict interseismic rates assumes fully homogeneous kinematic locking of the megathrust down to 35-km depth without along-strike variations, which is inconsistent with our observations and model of coupling coefficient (Figure 3) as well as with some previously published models (e.g., Li et al., 2015; Metois et al., 2016).

### 3. Results: Comparing Short-Term and Long-Term Uplift Rates

In contrast to previous analysis, we observe a slight correlation (Pearson product-moment correlation coefficient of 0.5) between the distribution of coupling coefficients offshore (i.e., 50-km offshore in the direction of convergence) and Quaternary uplift of the coastal domain (Figure 4). Quaternary uplift appears faster where coupling coefficient is high along the megathrust. However, because of the inherent limitations in inferred models of coupling (i.e., nonuniqueness), we rather rely on the relationship between predicted interseismic and long-term uplift. Effectively, as alluded to earlier, we consider our coupling model as no more than a physics-based interpolation, including uncertainties, of interseismic surface displacements along the coast. Although we do not include vertical GNSS-derived velocities in our inversion, a first-order comparison of the predicted interseismic uplift at available GNSS stations suggests a relatively correct agreement with our predictions (see supporting information and Blewitt et al., 2016). Such validation against an independent data set should be taken with caution as formal uncertainties in GNSS-derived velocities might be underestimated, especially for vertical rates of motion. In addition, we need to consider that numerous active faults have been recognized in the forearc, in particular over the regions of Tocopilla, Salar Grande, and North of Pisagua (Allmendinger & González, 2010). All types of faulting, reverse, normal, and strike slip, active over the Neogene and Quaternary have been identified in specific regions along the coastline, which could indicate along-strike variations in the long-term behavior of the forearc.

Plotting the interseismic, predicted, uplift rates with respect to the modeled Quaternary uplift rates, it appears that points can be separated in two groups (please refer to supporting information for a plot without our interpretation). Within each group, short-term and long-term rates correlate. After separating these points in two distinct groups, we find that there is a spatial coherence within these groups. In a first group (colored dots in Figure 4), we consider points from regions that have experienced extensive neogene and Quaternary active faulting according to Allmendinger and González (2010), while in the second group, we consider points from regions devoid of active faulting (black dots in Figure 4). Points are not randomly taken in a group or the other and rather cluster spatially along the coastline. Taken independently, the correlation between short-term and Quaternary uplift shows correlation coefficients of 0.74 and 0.76 for the areas with and without recent active faulting, respectively. While the separation might sound ad hoc at first, we believe that the spatial coherence of these two groups of points is the signature of an along-strike variable behavior of the forearc subjected to interseismic loading.

For a given interseismic uplift rate, estimates of long-term coastal uplift are consistently slower in areas that have experienced significant Quaternary faulting. We fit both data sets separately using a Bayesian regression technique (see supporting information) and infer the distribution of plausible linear relationships between Quaternary and short-term uplift. In both cases, we observe that inferred Quaternary uplift rates correspond to 4% to 8% of our estimated interseismic rates in northern Chile. In addition, it appears that, while a zero-valued interseismic uplift rate corresponds to a zero-valued Quaternary uplift rate for the regions affected by recent active faulting, this is not the case for regions without identified active faulting. In the later case, a zero-valued interseismic uplift rate corresponds to a  $0.1 \pm 0.05$  mm/year Quaternary uplift rate.

### 4. Discussion: Internal Anelastic Deformation and the Role of Faulting

We interpret the observed correlation(s) between million-year time scale uplift and present-day interseismic uplift as the long-term signature of interseismic deformation. We explain the distribution of short-term versus long-term uplift rates as the combination of three overlapping mechanisms. First, a broad regional scale

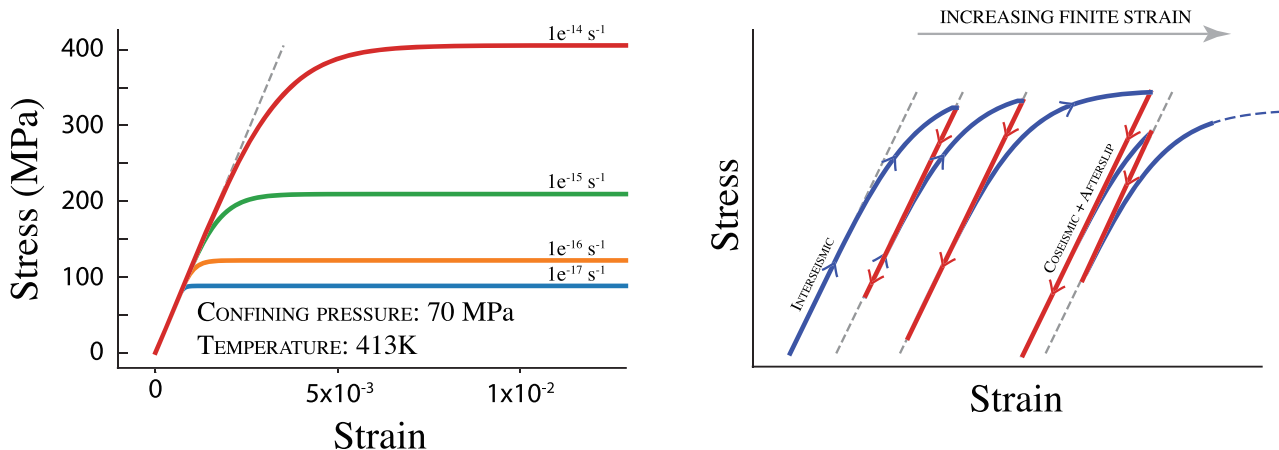


**Figure 5.** Schematic model for the accumulation of permanent strain throughout the earthquake cycle. (Left) Stress-strain relationship for the viscoplastic low-temperature deformation of quartz at 70 MPa and 413 K, conditions corresponding to a depth of about 7 km. As the viscoplastic response of quartz is strain rate dependent, we show the corresponding behavior for four strain rates corresponding to a range of interseismic strain rates. (Right) Schematic behavior of a viscoplastic material to the cycles of loading and unloading imposed by the succession of interseismic and coseismic phases on the megathrust. During the interseismic phase, stress increases in the forearc, at a strain rate imposed by the slip rate on the megathrust, hence the variable irrecoverable strain that builds up laterally. During the coseismic phase, stress drops to a lower level, leaving persistent strain within the forearc.

uplift of  $0.1 \pm 0.05$  mm/year affects the whole coastline in northern Chile. Second, 4% to 8% of the interseismic uplift is not balanced by coseismic and postseismic slip related to large megathrust earthquakes. Third, a systematic offset of about 0.1 mm/year is observed between regions that have and have not experienced active faulting over the Quaternary. Our interpretation therefore suggests that interseismic and coseismic deformations do not cancel each other over many cycles and that approximately 4% to 8% of the vertical interseismic uplift is permanent. While the imprint of fault locking on the forearc morphology has been previously hypothesized based on the trench parallel gravity anomaly (e.g., Song & Simons, 2003; Wells et al., 2003), we provide here a quantitative estimate of the amount of permanent deformation for northern Chile.

Then, two hypotheses could explain the systematic difference of uplift rates in regions with and without recent (neogene to Quaternary) active faulting. First, slip along shallow structures within the forearc may have dissipated part of the energy that should have transferred into gravitational potential energy (i.e., topography), hence a lesser efficiency at building topography. Second, the presence of such pervasive faulting could imply variations in forearc material properties along the coast. These hypotheses now need to be tested against in-depth modeling.

Essential to our interpretation is that forearc materials must deform beyond their elastic limit in between large megathrust earthquakes at characteristic interseismic strain rates of  $10^{-17}$  to  $10^{-15} \text{ s}^{-1}$  (i.e., 0.1 to 10 nanostrain per year) and upper crustal temperatures and pressures below  $\sim 400^\circ \text{C}$  and  $\sim 200 \text{ MPa}$ , respectively. Among possible candidate mechanisms, pressure solution processes enable viscous-like creep under low deviatoric stress and temperature, particularly in shallow porous rock units (e.g., sedimentary layers) (Niemeijer et al., 2002). Under greater deviatoric stresses, low-porosity rocks are more likely to deform inelastically through brittle creep—the macroscopic manifestation of grain-scale cracks that nucleate from preexisting defects and grow subcritically through stress-activated and temperature-activated chemical processes (Brantut et al., 2013; Paterson & Wong, 2005).

We illustrate the possible behavior of the forearc through the example of quartz, a material typical of a continental crust, which can deform viscoplastically through dislocation glide at low temperature (Bhat et al., 2011). Under a compressive load, such material behaves elastically at low-strain regime and starts to deviate from elasticity at higher strain, and the style of deformation (i.e., elastic or inelastic) depends on the ambient strain rate (Figure 5). For strain rates on the order of those expected for the interseismic period within the forearc (i.e.,  $10^{-17}$  to  $10^{-15} \text{ s}^{-1}$ ), quartz behaves elastically for stresses lower than about 100 MPa, with inelastic strain increasing at higher stresses. Such a viscoplastic material would allow for interseismic loading up to absolute stresses on the order of those of a typical stress drop (i.e., less than 100 MPa), while accumulating permanent strain. In addition, because quartz tends to be elastic at high strain rates, we can

assume that the forearc would behave elastically during the coseismic (and maybe immediate postseismic) period.

Our interpretation focuses only on the behavior of the upper crust of the overriding plate and thus does not account for the viscous rheology of the upper mantle over the earthquake cycle (Wang et al., 2012), which may affect surface strain rates and estimates of coupling along the megathrust (Li et al., 2015). Also, we do not account for other potential transient deformation events. Postseismic stress relaxation following large earthquakes, for instance, occurs through aseismic slip (e.g., Hsu et al., 2006) and viscous flow within the upper mantle (e.g., Trubienko et al., 2013). The influence of mantle relaxation considering a crust that can deform inelastically has not been extensively modeled yet. That said, we believe that accounting for viscous processes in the mantle and afterslip would not modify our conclusions based purely on the comparison of surface deformation. First, given the geological time scales required to build topography, we can consider large earthquakes and their corresponding afterslip as single slip events. Second, postseismic viscous flow within the upper mantle following a large earthquake puts the forearc in compression for a period of time that depends on the characteristic time involved (Sun et al., 2014). If that characteristic time is small with respect to large megathrust cycles, it should be negligible.

Other examples worldwide do not necessarily compare simply with the behavior we observe in northern Chile. For instance, in Japan, the coastline of Tohoku subsides both during large earthquakes (e.g., Simons et al., 2011) and during the interseismic period (e.g., Hu et al., 2016). Only during the postseismic period, a selection of GNSS-derived ground velocities indicates uplift of the forearc. Although all phases of the earthquake cycle have been recorded in this region, the summation of observed coseismic, modeled postseismic and observed interseismic motion cannot explain the long-term uplift observed in the area. Viscoelastic models of interseismic motion allow for a potential reversal of rates of vertical motion during the interseismic period (Hashima & Sato, 2017; Trubienko et al., 2013), which could reconcile long-term and short-term observations in this part of Japan. In northern Chile, the only available surface deformation measurements are during the interseismic period and for moderate sized earthquakes and their respective postseismic sequences. Considering the example of Tohoku, surface displacements related to the largest possible event (and its postseismic displacements) along the megathrust completely override signals from other smaller magnitude events. Therefore, a complete budget of vertical displacements is impossible here, and we can only hypothesize based on the observed correlation. Systematic mapping of short-term and long-term vertical motion of subduction forearcs is therefore required to determine globally how much of plate convergence actually ends up in permanent deformation of subduction forearcs worldwide in order to constrain future geodynamical models attempting at bridging time scales, from seconds to millions of years.

#### Acknowledgments

This project has received funding from NASA (Grant NNX16AK58G). This project has received funding from the European Research Council (ERC) under the European Union's Horizon 2020 research and innovation program (Grant Agreements 758210 and 805256). This work was granted access to the HPC resources of MesoPSL financed by the Region Ile de France and the project Equip@Meso (reference ANR-10-EQPX-29-01) of the program Investissements d'Avenir supervised by the Agence Nationale pour la Recherche. Envisat raw data have been obtained upon request via the EOLISA tool. We thank the European Space Agency for the acquisition and the distribution of these data. ERA-Interim products are directly available for download at ECMWF (<https://www.ecmwf.int/>). The authors are grateful for enlightening discussions with J.-P. Avouac, N. Cubas, L. Dal Zilio, and N. Brantut. The authors thank the editor and both an anonymous reviewer and R. Bürgmann for their constructive comments that helped craft a better manuscript.

#### References

- Allmendinger, R. W., & González, G. (2010). Invited review paper: Neogene to Quaternary tectonics of the Coastal Cordillera, northern Chile. *Tectonophysics*, 495(1-2), 93–110.
- Baker, A., Allmendinger, R. W., Owen, L. A., & Rech, J. A. (2013). Permanent deformation caused by subduction earthquakes in northern Chile. *Nature Geoscience*, 6(5), 492–496.
- Bejar-Pizarro, M., Carrizo, D., Socquet, A., Armijo, R., Barrientos, S., Bondoux, F., et al. (2010). Asperities and barriers on the seismogenic zone in North Chile: State-of-the-art after the 2007 Mw 7.7 Tocopilla earthquake inferred by GPS and InSAR data. *Geophysical Journal International*, 183, 390–406. <https://doi.org/10.1111/j.1365-246X.2010.04748.x>
- Bejar-Pizarro, M., Socquet, A., Armijo, R., Carrizo, D., Genrich, J., & Simons, M. (2013). Andean structural control on interseismic coupling in the North Chile subduction zone. *Nature Geoscience*, 6(5), 462–467.
- Bhat, H. S., Sammis, C. G., & Rosakis, A. J. (2011). The micromechanics of Westerley granite at large compressive loads. *Pure and Applied Geophysics*, 168(12), 2181–2198.
- Blewitt, G., Kreemer, C., Hammond, W. C., & Gazeaux, J. (2016). MIDAS robust trend estimator for accurate GPS station velocities without step detection. *Journal of Geophysical Research: Solid Earth*, 121, 2054–2068. <https://doi.org/10.1002/2015JB012552>
- Brantut, N., Heap, M. J., Meredith, P. G., & Baud, P. (2013). Time-dependent cracking and brittle creep in crustal rocks: A review. *Journal of Structural Geology*, 52(C), 17–43.
- Comte, D., & Pardo, M. (1991). Reappraisal of great historical earthquakes in the northern Chile and southern Peru seismic gaps. *Natural Hazards*, 4(1), 23–44.
- Davis, D. M., Suppe, J., & Dahlen, F. A. (1983). Mechanics of fold-and-thrust belts and accretionary wedges. *Journal of Geophysical Research*, 88(B2), 1153–1172.
- Dragert, H., Wang, K., & Thomas, J. S. (2001). A silent slip event on the deeper Cascadia subduction interface. *Science*, 292(5521), 1525–1528.
- Duputel, Z., Jiang, J., Jolivet, R., Simons, M., Rivera, L., Ampuero, J. P., et al. (2015). The Iquique earthquake sequence of April 2014: Bayesian modeling accounting for prediction uncertainty. *Geophysical Research Letters*, 42, 7949–7957. <https://doi.org/10.1002/2015GL065402>
- Ekström, G., Nettles, M., & Dziewonski, A. M. (2012). The global CMT project 2004–2010: Centroid-moment tensors for 13,017 earthquakes. *Physics of the Earth and Planetary Interiors*, 200–201(0), 1–9.

- Farr, T. G., & Kobrick, M. (2000). Shuttle radar topography mission produces a wealth of data. *Eos, Transactions American Geophysical Union*, 81(48), 583–585.
- Freymueller, J. T., & Beavan, J. (1999). Absence of strain accumulation in the Western Shumagin Segment of the Alaska Subduction Zone. *Geophysical Research Letters*, 26(21), 3233–3236. <https://doi.org/10.1029/1999GL008356>
- Grandin, R., Klein, E., Metois, M., & Vigny, C. (2016). Three-dimensional displacement field of the 2015  $M_w$ 8.3 Illapel earthquake (Chile) from across- and along-track Sentinel-1 TOPS interferometry. *Geophysical Research Letters*, 43, 2552–2561. <https://doi.org/10.1002/2016GL067954>
- Hashima, A., & Sato, T. (2017). A megathrust earthquake cycle model for northeast Japan: Bridging the mismatch between geological uplift and geodetic subsidence. *Earth Planets Space*, 69(1), 1–10.
- Hirose, H., Hirahara, K., Kimata, F., Fujii, N., & Miyazaki, S. (1999). A slow thrust slip event following the two 1996 Hyuganada earthquakes beneath the Bungo Channel, southwest Japan. *Geophysical Research Letters*, 26(21), 3237–3240.
- Hsu, Y.-J., Simons, M., Avouac, J.P., Galetzka, J., Sieh, K., Chlieh, M., et al. (2006). Frictional afterslip following the 2005 Nias-Simeulue earthquake, Sumatra: Supplementary material. *Science*, 312(5782), 1921–1925.
- Hu, Y., Bürgmann, R., Uchida, N., Banerjee, P., & Freymueller, J. T. (2016). Stress-driven relaxation of heterogeneous upper mantle and time-dependent afterslip following the 2011 Tohoku earthquake. *Journal of Geophysical Research: Solid Earth*, 121, 385–411. <https://doi.org/10.1002/2015JB012508>
- Jolivet, R., & Simons, M. (2018). A multipixel time series analysis method accounting for ground motion, atmospheric noise, and orbital errors. *Geophysical Research Letters*, 45, 1814–1824. <https://doi.org/10.1002/2017GL076533>
- Jolivet, R., Simons, M., Agram, P. S., Duputel, Z., & Shen, Z. K. (2015). Aseismic slip and seismogenic coupling along the central San Andreas Fault. *Geophysical Research Letters*, 42, 297–306. <https://doi.org/10.1002/2014GL062222>
- Konca, A. O., Avouac, J.-P., Sladen, A., Meltzner, A. J., Sieh, K., Fang, P., et al. (2008). Partial rupture of a locked patch of the Sumatra megathrust during the 2007 earthquake sequence. *Nature*, 456(7222), 631–635.
- Li, S., Moreno, M., Bedford, J., Rosenau, M., & Oncken, O. (2015). Revisiting viscoelastic effects on interseismic deformation and locking degree: A case study of the Peru-North Chile subduction zone. *Journal of Geophysical Research: Solid Earth*, 120, 4522–4538. <https://doi.org/10.1002/2015JB011903>
- Lin, Y. N., Jolivet, R., Simons, M., Agram, P. S., Martens, H. R., Li, Z., & Lodi, S. H. (2015). High interseismic coupling in the Eastern Makran (Pakistan) subduction zone. *Earth and Planetary Science Letters*, 420(C), 116–126.
- Matsu'ura, T. (2015). Late Quaternary uplift rate inferred from marine terraces, Muroto Peninsula, southwest Japan: Forearc deformation in an oblique subduction zone. *Geomorphology*, 234(C), 133–150.
- Mazzotti, S., Le Pichon, X., Henry, P., & Miyazaki, S.-I. (2000). Full interseismic locking of the Nankai and Japan-west Kurile subduction zones: An analysis of uniform elastic strain accumulation in Japan constrained by permanent GPS. *Journal of Geophysical Research*, 105(B6), 13,159–13,177.
- Melnick, D. (2016). Rise of the central Andean coast by earthquakes straddling the Moho. *Nature Geoscience*, 9(5), 401–407.
- Metois, M., Socquet, A., Vigny, C., Carrizo, D., Peyrat, S., Delorme, A., et al. (2013). Revisiting the North Chile seismic gap segmentation using GPS-derived interseismic coupling. *Geophysical Journal International*, 194(3), 1283–1294.
- Metois, M., Vigny, C., & Socquet, A. (2016). Interseismic coupling, megathrust earthquakes and seismic swarms along the Chilean subduction zone ( $38^{\circ}$ – $18^{\circ}$ S). *Pure and Applied Geophysics*, 173, 1431–1449.
- Mouslopoulou, V., Oncken, O., Hainzl, S., & Nicol, A. (2016). Uplift rate transients at subduction margins due to earthquake clustering. *Tectonics*, 35, 2370–2384. <https://doi.org/10.1002/2016TC004248>
- Niemeijer, A. R., Spiers, C. J., & Bos, B. (2002). Compaction creep of quartz sand at 400–600°C: Experimental evidence for dissolution-controlled pressure solution. *Earth and Planetary Science Letters*, 195(3-4), 261–275.
- Nocquet, J. M., Villegas-Lanza, J. C., Chlieh, M., Mothes, P. A., Rolandone, F., Jarrin, P., et al. (2014). Motion of continental slivers and creeping subduction in the northern Andes. *Nature Geoscience*, 7(4), 287–291.
- Paterson, M. S., & Wong, T.-f. (2005). *Experimental rock deformation—The brittle field*. Berlin/Heidelberg: Springer-Verlag.
- Pritchard, M., Simons, M., Rosen, P. A., Hensley, S., & Webb, F. H. (2002). Co-seismic slip from the 1995 July 30  $Mw$ =8.1 Antofagasta, Chile, earthquake as constrained by InSAR and GPS observations. *Geophysical Journal International*, 150, 362–376.
- Pritchard, M. E., Ji, C., & Simons, M. (2006). Distribution of slip from 11  $Mw$ > 6 earthquakes in the northern Chile subduction zone. *Journal of Geophysical Research*, 111, B10302. <https://doi.org/10.1029/2005JB004013>
- Pritchard, M. E., & Simons, M. (2002). A satellite geodetic survey of large-scale deformation of volcanic centres in the central Andes. *Nature*, 418(6894), 167–171.
- Ramírez-Herrera, M. T., Gaidzik, K., Forman, S., Kostoglodov, V., Bürgmann, R., & Johnson, C. W. (2018). Relating the long-term and short-term vertical deformation across a transect of the forearc in the central Mexican subduction zone. *Geosphere*, 14(2), 419–439.
- Regard, V., Saillard, M., Martinod, J., Audin, L., Carretier, S., Pedoja, K., et al. (2010). Renewed uplift of the central Andes forearc revealed by coastal evolution during the Quaternary. *Earth and Planetary Science Letters*, 297(1-2), 199–210.
- Rousset, B., Lasserre, C., Cubas, N., Graham, S., Radiguet, M., DeMets, C., et al. (2015). Lateral variations of interplate coupling along the Mexican subduction interface: Relationships with long-term morphology and fault zone mechanical properties. *Pure and Applied Geophysics*, 173(10), 3467–3486.
- Saillard, M., Audin, L., Rousset, B., Avouac, J. P., Chlieh, M., Hall, S. R., et al. (2017). From the seismic cycle to long-term deformation: Linking seismic coupling and Quaternary coastal geomorphology along the Andean megathrust. *Tectonics*, 36, 241–256. <https://doi.org/10.1002/2016TC004156>
- Saillard, M., Hall, SR, Audin, L., Farber, DL, Héral, G, Martinod, J., et al. (2009). Non-steady long-term uplift rates and Pleistocene marine terrace development along the Andean margin of Chile ( $31^{\circ}$ S) inferred from  $^{10}\text{Be}$  dating. *Earth and Planetary Science Letters*, 277(1-2), 50–63.
- Savage, J. C. (1983). A dislocation model of strain accumulation and release at a subduction zone. *Journal of Geophysical Research*, 88(B6), 4984–4996.
- Schurr, B., Asch, G., Hainzl, S., Bedford, J., Hoechner, A., Palo, M., et al. (2014). Gradual unlocking of plate boundary controlled initiation of the 2014 Iquique earthquake. *Nature*, 512(7514), 1–13.
- Schurr, B., Asch, G., Rosenau, M., Wang, R., Oncken, O., Barrientos, S., et al. (2012). The 2007  $M_7.7$  Tocopilla northern Chile earthquake sequence: Implications for along-strike and downdip rupture segmentation and megathrust frictional behavior. *Journal of Geophysical Research*, 117, B05305. <https://doi.org/10.1029/2011JB009030>
- Simons, M., Galetzka, J., Genrich, JF, Ortega Culaciati, F., Comte, D., Glass, B., et al. (2010). Central Andean Tectonic Observatory Geodetic Array. UNAVCO Inc.

- Simons, M., Minson, S. E., Sladen, A., Ortega, F., Jiang, J., Owen, S. E., et al. (2011). The 2011 magnitude 9.0 Tohoku-Oki earthquake: Mosaicking the megathrust from seconds to centuries. *Science*, 332(6036), 1421–1425.
- Song, T.-R. A., & Simons, M. (2003). Large trench-parallel gravity variations predict seismogenic behavior in subduction zones. *Science*, 301(5633), 630–633.
- Sun, T., Wang, K., Iinuma, T., Hino, R., He, J., Fujimoto, H., et al. (2014). Prevalence of viscoelastic relaxation after the 2011 Tohoku-Oki earthquake. *Nature*, 514(7520), 1–13.
- Trubienko, O., Fleitout, L., Garaud, J.-D., & Vigny, C. (2013). Interpretation of interseismic deformations and the seismic cycle associated with large subduction earthquakes. *Tectonophysics*, 589, 126–141.
- Victor, P., Sobiesiak, M., Glodny, J., Nielsen, S. N., & Oncken, O. (2011). Long-term persistence of subduction earthquake segment boundaries: Evidence from Mejillones Peninsula, northern Chile. *Journal of Geophysical Research*, 116, B02402. <https://doi.org/10.1029/2010JB007771>
- Vigny, C., Socquet, A., Peyrat, S., Ruegg, J. C., Metois, M., Madariaga, R., et al. (2011). The 2010 Mw 8.8 Maule megathrust earthquake of central Chile, monitored by GPS. *Science*, 332(6036), 1417–1421.
- Wang, K., Hu, Y., & He, J. (2012). Deformation cycles of subduction earthquakes in a viscoelastic Earth. *Nature*, 484(7394), 327–332.
- Wells, R. E., Blakely, R. J., Sugiyama, Y., Scholl, D. W., & Dinterman, P. A. (2003). Basin-centered asperities in great subduction zone earthquakes: A link between slip, subsidence, and subduction erosion? *Journal of Geophysical Research*, 108(B10), 2507. <https://doi.org/10.1029/2002JB002072>